Dielectric Properties of Water inside Single-Walled Carbon Nanotubes

Fuminori Mikami,[†] Kazuyuki Matsuda,[†] Hiromichi Kataura,[‡,§] and Yutaka Maniwa[†,§,*]

[†]Department of Physics, Faculty of Science, Tokyo Metropolitan University, 1-1 Minami-osawa, Hachioji, Tokyo 192-0397, Japan, [‡]Nanotechnology Institute, National Institute of Advanced Industrial Science and Technology (AIST), Tsukuba 305-8562, Japan, and [§]JST, CREST, Kawaguchi, 332-0012, Japan

ABSTRACT In this paper, we report novel ferroelectric properties of a new form of ice inside single-walled carbon nanotubes (SWCNTs). These are called "ice nanotubes" (ice NTs) and they consist of polygonal water rings stacked one-dimensionally along the SWCNT axis. We performed molecular dynamics (MD) calculations for the ice NTs under an external electric field and in a temperature range between 100 and 350 K. It is revealed that ice NTs show stepwise polarization with a significant hysteresis loop as a function of the external field strength. In particular, pentagonal and heptagonal ice NTs are found to be the world's smallest ferroelectrics with spontaneous polarization of around 1 $\mu C/cm^2$. The n-gonal ice NT, where $n = 5$, 6, or 7, has $(n + 1)$-polarized structures with different polarizations. These findings suggest potential applications of SWCNTs encapsulating dielectric materials for the fabrication of the smallest ferroelectric devices. Experimental evidence for the presence of ice NTs inside SWCNTs is also discussed in great detail.

KEYWORDS: carbon nanotubes · ferroelectric · water · ice nanotubes · dielectric property

Water molecules have a permanent electric dipole moment of 1.8546 debye.[1] Ferroelectricity can thus be expected to be induced when the water molecules condense into a solid form. Bulk ice, however, is usually not ferroelectric because of proton disorder.[1] From this viewpoint, strongly confined water inside a small cavity is very interesting because new novel structures of water can be formed.[2] Here, we assess the dielectric properties of water confined inside single-walled carbon nanotubes (SWCNTs) with a finite length by employing classical molecular dynamics (MD) calculations in the presence of an external electric field.

SWCNTs are seamless tubes made of graphene sheets, and they have a one-dimensional cavity with diameter ranging from subnanometer dimensions to a few nanometers.[3,4] In spite of the hydrophobic nature of the SWCNT wall, it is known from experimental[5−9] and theoretical[10−12] studies that water can be adsorbed inside SWCNTs without the application of a high-pressure if the SWCNTs are heat-treated in air to open the wall. Such strongly confined water inside SWCNTs has been extensively investigated theoretically.[10−22] One of the interesting predictions from these studies is the formation of a new form of water with a tube-like structures at low temperatures, the so-called ice nanotubes (ice-NTs).[15] The existence of ice-NTs was experimentally confirmed in SWCNTs with diameters between 1.1 and 1.5 nm.[6,11,23] Multilayer water tubes were also discussed in theoretical calculations in larger diameter SWCNTs.[21,22] In the intermediate SWCNT diameter range, ranging from 1.4 to 1.5 nm, an ice-NT like structure containing a one-dimensional water chain was described.[24,22]

Because of the peculiar structures of ice-NTs with respect to proton arrangement in water, the dielectric properties of water inside SWCNTs are particularly interesting.[15,16,18,19,25,26] Theoretical calculations on single layer ice-NTs indicate that each one-dimensional chain along the SWCNT axis, which consists of ice-NTs, is proton-ordered along the SWCNT axis, that is, each chain in the ice-NTs is a proton-ordered ferroelectric at the lowest energy state. On the other hand, interchain coupling between these ferroelectric chains is believed to be antiferroelectric.

In real systems, however, the one-dimensional nature of the SWCNT cavity should be another factor to determine the dielectric properties. It may cause large amplitude long-range fluctuations, and does not allow the formation of long-range order at finite temperatures.[27−29] An NMR experiment using an SWCNT sample with an average diameter of 1.35 nm indicated that all the large amplitude proton dynamics in ice-NTs are frozen below 120 K within the NMR time scale of 10^{-5} s.[25] However, little is known about the dielectric properties of

*Address correspondence to maniwa@phys.metro-u.ac.jp.

Received for review March 5, 2009 and accepted April 09, 2009.

Published online April 22, 2009.
10.1021/nn900221t CCC: $40.75

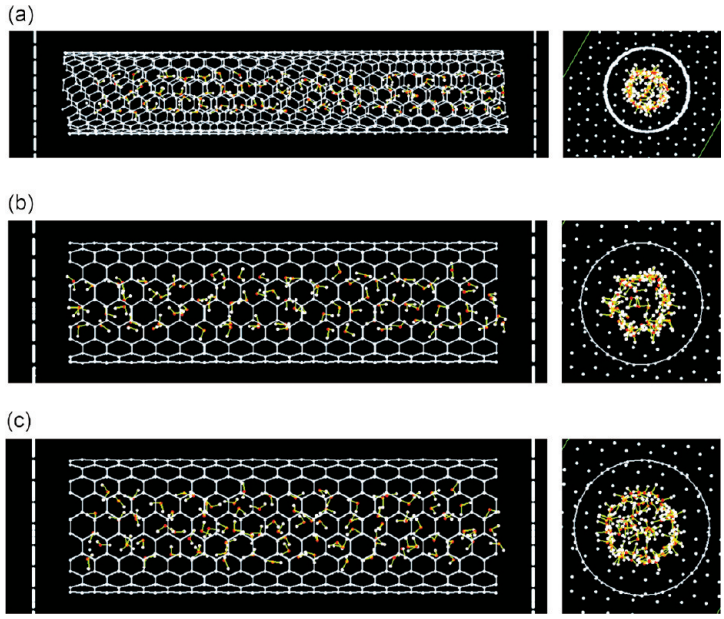

Figure 1. The water-SWCNT systems examined in this study. (a) (9,8) SWCNT encapsulating 104 TIP3P water molecules. (b) (9,9) SWCNT encapsulating 83 TIP3P water molecules. (c) (10,10) SWCNT encapsulating 98 TIP3P water molecules. Flat walls made of artificial atoms are located at both edges of SWCNT to prevent water from escaping from the inside of the SWCNTs.

ice-NTs thus far. We have therefore carried out a systematic investigation of confined water inside SWCNTs *as dielectrics* by means of molecular dynamics (MD) calculations *in the presence of zero and finite electric fields* along the SWCNT axis.

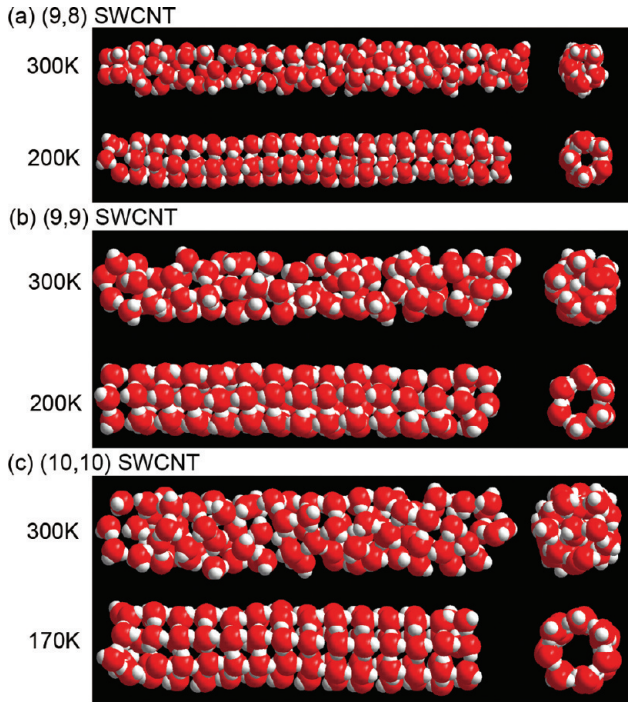

Figure 2. Snapshot structures of water inside (a) the (9,8) SWCNT, (b) the (9,9) SWCNT, and (c) the (10,10) SWCNT at high and low temperatures. Left: side views. Right: top views. The low temperature structures are pentagonal, hexagonal, and heptagonal ice-NTs for panels a, b, and c, respectively. The ice-NTs consist of proton-ordered one-dimensional water chains at low temperature. The small white spheres are positively charged hydrogen atoms. The large red spheres are negativity charged oxygen atoms.

TABLE 1. Simulated SWCNT Systems Encapsulating Water Molecules

SWCNT index	diameter nm	length nm	number of H_2O
(9,8)	1.153	6.2, 12.4	104,208
(9,9)	1.221	4.3	83
(10,10)	1.356	4.3	98

RESULTS AND DISCUSSION

Classical molecular dynamics (MD) calculations were performed on water encapsulated in *finite length* SWCNTs with indexes (9,8), (9,9), and (10,10). The MD calculations were performed using the software package Materials Explorer 5.0 (Fujitsu Ltd.). The number of confined water molecules and the SWCNT lengths and diameters are listed in Table 1.

The TIP3P water model[30,31] was chosen to describe the water molecules, which consist of an oxygen atom with a negative charge and two hydrogen atoms with a positive charge. The TIP3P water has a permanent electric dipole moment of $p_w = 2.35$ debye $= 7.84 \times 10^{-30}$ C · m. The systems presented in this paper are illustrated in Figure 1. To ensure encapsulation of water inside SWCNTs during the calculations even before achieving thermal equilibrium and even at higher temperatures, flat walls made of artificial atoms are located 0.3 nm from both the SWCNT edges. SWCNTs and the artificial atoms are fixed, and TIP3P water is treated as a rigid body; internal degrees of freedoms within the water molecule are not included.

First, we discuss the results in a zero electric field for the three systems mentioned above. The number of water molecules encapsulated are 104, 83, and 98 for the (9,8), (9,9), and (10,10) SWCNTs, respectively.[32] Snapshots of structures obtained at high temperature (300 K) and low temperatures (200 or 170 K) are shown as examples in Figure 2. In the simulations, the temperature was first held for more than 1 ns at a temperature higher than 300 K, then ramped down to 200 K or below at a rate 12.5 K/ns for the (9,8) and (9,9) SWCNTs and 5.41 K/ns for the (10,10) SWCNT. A faster temperature variation of 50 K/ns, was also examined, but essentially the same results were obtained. In Figure 2, we observe that pentagonal, hexagonal, and heptagonal ice-NTs are formed at low temperatures for the (9,8), (9,9), and (10,10) SWCNT systems, respectively. Similar results have been reported in previous papers, wherein the calculations were performed under periodic boundary conditions using different water models, TIP4P or SPC/E.[15,10,20]

As shown in Figure 2, the ice-NT structures consist of *n*-gonal water rings stacked one-dimensionally along the SWCNT axis, where *n* is an integer, that is, $n = 5$, 6, and 7

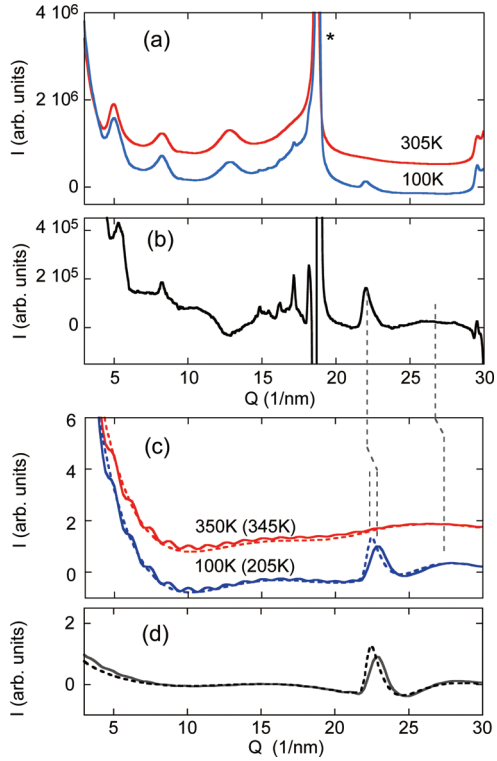

Figure 3. Experimentally observed and simulated X-ray diffraction (XRD) patterns in the thinner SWCNT systems. (a) XRD patterns of water-adsorbing bundles consisting of SWCNTs with a mean diameter of 1.17 nm at 305 (upper) and 100 K (lower).[23] (b) Difference between the XRD patterns taken at high and low temperatures in panel a. (c) Calculated interference function, I_{oo}, at high and low temperatures in the (9,8) SWCNT systems. The solid lines are for the short SWCNT system with 104 water molecules, and the dotted lines are for the longer SWCNT system with 208 water molecules. The temperatures given in parentheses are for the longer SWCNT system. (d) Difference in $I_{OO}(Q)$ in panel c. The asterisk (*) denotes the Bragg peak of a graphite impurity. The data are shifted to distinguish between them. The vertical dotted lines are shown as a guide to the eye.

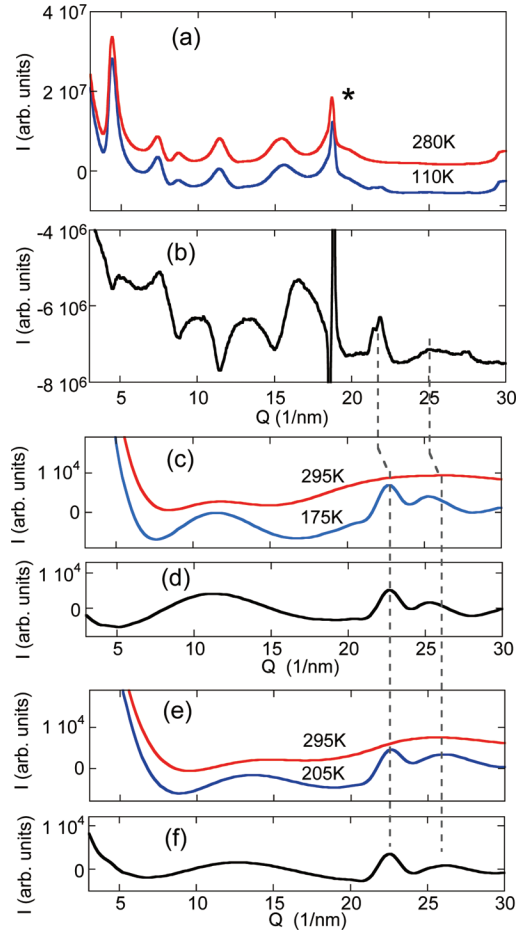

Figure 4. Experimentally observed and simulated X-ray diffraction (XRD) patterns in the thicker SWCNT systems. (a) XRD patterns of water-adsorbing bundles consisting of SWCNTs with a mean diameter of 1.35 nm at 280 K (upper) and 110 K (lower). (b) Difference in the XRD patterns in panel a. (c and e) Calculated interference function, I_{oo}, at high and low temperatures in the (10,10) and (9,9) SWCNT systems, respectively. (d and f) Difference in I_{oo} in panels c and e, respectively. From a comparison of the real XRD patterns with simulated ones, it is suggested that both the heptagonal and hexagonal ice-NTs are formed in the real SWCNT sample because of the diameter distribution in the real SWCNT sample. Octagonal ice-NT has also been suggested to exist in the sample.[23] The asterisk (*) denotes the Bragg peak of a graphite impurity. The data are shifted to distinguish between them. The vertical dotted lines are shown as a guide to the eye.

for pentagonal, hexagonal, and heptagonal ice-NTs, respectively. The structures can also be seen as a polygon tube consisting of n one-dimensional water chains aligned parallel to each other through hydrogen bonds. It should be emphasized that one of the oxygen-proton bonds within each water chain is ordered along the SWCNT axis, except for the edge molecules of ice-NTs.

To check the reliability of the present simulations in reproducing experimental results,[6,23] X-ray interference functions, I_{OO}, between oxygen−oxygen (O−O) atoms in water were calculated at several temperatures using a built-in tool in the software package and compared with the experimental results. Here, I_{ij} between i and j atoms is defined as

$$I_{ij}(Q) = \frac{w_i f_i w_j f_j}{|\sum_k w_k f_k|^2} \times \frac{N}{V} \int_0^{r_m} [g_{ij}(r) - 1] \frac{\sin(Qr)}{Qr} 4\pi r^2 \, dr \quad (1)$$

$Q = 4\pi \sin\theta / \lambda$ where Q is the amplitude of X-ray scattering vector, 2θ is the scattering angle, λ is the X-ray wavelength, N is the total number of atoms, V is the system volume, $w_i (= N_i/N)$ is the partial number of atom i, f_i is the atomic scattering factor for atom i, and $g_{ij}(r)$ is the distribution function between i and j atoms. The X-ray interference functions are related to the X-ray diffraction pattern as

$$I(Q) \propto \sum_{i,j} I_{ij}(Q) \quad (2)$$

In an earlier paper,[10] following Gnutzmann and Vogel,[33] Striolo *et al.* characterized the snapshot struc-

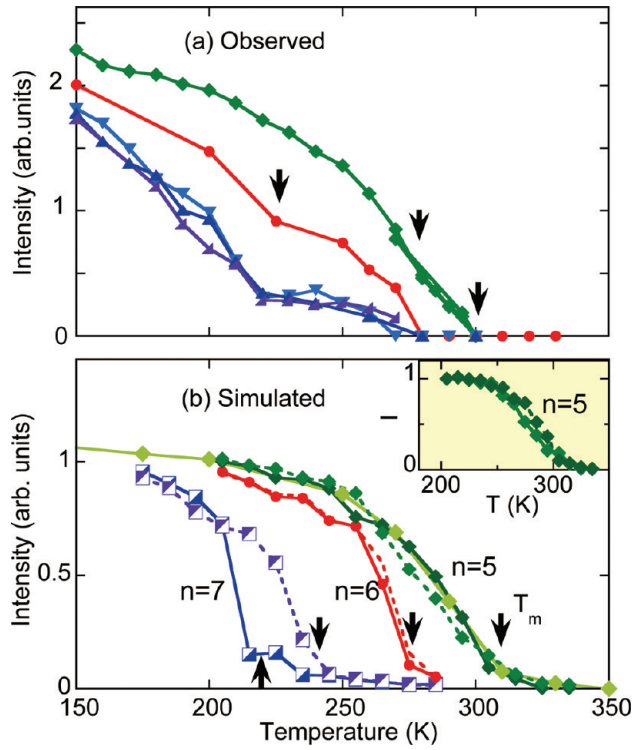

Figure 5. Temperature dependence of the Bragg peak intensity at $Q \approx 22$ nm^{-1}. (a) Experimentally observed peak intensity in five SWCNT specimens with different mean diameters covering 1.0−1.5 nm.[23] (b) Simulated XRD peak intensity at $Q \approx 22$ nm^{-1} due to the pentagonal ($n = 5$), hexagonal ($n = 6$), and heptagonal ($n = 7$) ice-NTs. The arrows define the formation temperatures of ice-NTs, T_m. The dotted lines are for increasing temperature. The solid lines are for decreasing temperature. The inset shows the normalized intensity at 200 K for the longer (9,8) system with 208 water molecules.

tures of water confined inside SWCNTs by using the Debye function:

$$I(Q) = \sum_{i,j} f_i f_j \frac{\sin(Qr_{ij})}{Qr_{ij}} \qquad (3)$$

Comparing with eq 1, the summation in eq 3 is replaced by the integration of $g_{ij}(r)$ in eq 1. Although there is an additional term in the integration in eq 1, the two equations are essentially the same to describe the main characteristics of the X-ray diffraction pattern.

The calculated I_{OO} for the 104 water molecules inside the (9,8) SWCNT at 350 and 100 K is shown by solid lines in Figure 3c. For the (10,10) and (9,9) SWCNT systems, I_{OO} at high and low temperatures is given in Figure 4 panels c and e, respectively. For these three systems, we find that a new peak in $I_{OO}(Q)$ appears at $Q \approx 22$ nm^{-1} at lower temperatures. The corresponding periodicity, $2\pi/Q$, is about 0.28 nm, close to the hydrogen bond length in bulk ice, and can be definitely assigned to the periodic structure of the one-dimensional array of polygonal water rings in the ice-NTs. Simultaneous with the appearance of this peak with lowering temperature, an oscillatory behavior appears in $I_{OO}(Q)$ in a wide Q region below 20 nm^{-1}. This oscillation is more clearly observed in the thicker (9,9) and (10,10) SWCNTs than in the (9,8) SWCNT system, and is particularly obvious in the difference in $I_{OO}(Q)$ between the high and low temperatures, as seen in Figures 3d, 4d,f. This oscillation is presumably caused by the rearrangement of water into a tube-like structure at low temperatures, as demonstrated in the top views of the SWCNT systems in Figure 2.

The peak intensity at $Q \approx 22$ nm^{-1}, I_{OO} (22), develops with temperature as shown in Figure 5b. Defining the onset temperature of ice-NT formation, T_m, as shown by the arrows in Figure 5b, we have $T_m = 310 \pm 5$ K for the pentagonal ice-NT in the (9,8) SWCNT and 275 ± 5 K for the hexagonal ice-NT in the (9,9) SWCNT. By contrast the heptagonal ice-NT in the thicker (10,10) SWCNT exhibits a large hysteresis; $T_m = 220 \pm 5$ K for lowering temperature and 240 ± 5 K for rising temperature. The size dependence of T_m was also examined for the case of the (9,8) SWCNT system. The inset in Figure 5b shows the temperature dependence for the longer (9,8) SWCNT with 208 water molecules. Compared with the result for the shorter SWCNT, T_m is almost the same for both.

The corresponding X-ray diffraction (XRD) patterns of the real SWCNT samples are shown in Figure 3a for the SWCNT specimen with a mean diameter of 1.17 nm and in Figure 4a for the SWCNT specimen with a mean diameter of 1.35 nm.[23] In the XRD patterns in the earlier report,[6] there were extrinsic peaks due to bulk ice inside and outside the XRD glass capillary containing the SWCNT samples. In contrast, the XRD patterns in this study contain almost no signal from bulk water because the measurements and the water adsorption treatment were carefully carried out under well-controlled conditions. The present XRD experiments were performed using synchrotron radiation X-rays with a wavelength of 0.10 nm at the BL1B station of the KEK PF facility.

Comparing the simulated and the observed patterns, it must be noted that the simulated patterns lack the experimentally observed Bragg peaks rising from the bundle structure of the SWCNTs. These Bragg peaks appear dominantly below $Q \approx 20$ nm^{-1}. This is because the simulations were carried out on single isolated SWCNTs encapsulating the water molecules. Therefore, we focus our attention on the XRD profiles above $Q \approx 20$ nm^{-1} in the present paper. Some effects of water-rearrangement on the bundle Bragg peaks have been discussed in the earlier report.[6]

From Figures 3a and 4a for the observed raw XRD patterns and Figures 3b and 4b for differences between high and low temperatures, we observe the appearance of new Bragg peaks at $Q \approx 22$ nm^{-1} at low temperatures in both samples. The peak profile has an oscillatory tail in the higher Q direction (>22 nm^{-1}). The period of oscillation seems to be shorter in the 1.35 nm diameter SWCNTs than in the 1.17 nm diameter

SWCNTs. All of these features observed in the experiments agree well with the simulated patterns in Figures 3c,d and 4c−f. The observed tail is a characteristic of the one-dimensionality of the ice-NT structures and its oscillation is related to the diameter of the water polygon in ice-NTs. A detailed comparison suggests that the pentagonal ice-NT is dominantly formed inside the 1.17 nm diameter SWCNT specimen. In the 1.35 nm SWCNT specimen, on the other hand, the observed high-Q tail seems to be between that for the hexagonal and the heptagonal ice-NTs, so that it is a mix of the hexagonal and the heptagonal ice-NTs. This likely occurs because the SWCNT specimen used for the measurements inevitably has a diameter distribution (about 0.2 nm).

By a more detailed comparison, however, we notice that the width of the simulated peaks is substantially larger, and the peak position shifts slightly toward the high-Q direction. Such discrepancies can definitely be ascribed to the smaller crystalline (or system) size used in the simulations. Indeed, this can be confirmed by an additional calculation for the larger system with 208 water molecules inside the longer (9,8) SWCNT. These results are shown by the dotted lines in Figure 3c,d; the peak becomes sharper and shifts to a lower Q direction compared to the shorter SWCNT system with 104 water molecules, so that we obtain better agreement with the experiments. This implies, in reverse, that the domain sizes of the ice-NTs in real systems should be much larger than 20 polygon units; in the case of pentagonal ice NT, for example, it would be about 40 units.

The temperature dependence of the peak intensity, I_{OO} (22), is summarized in Figure 5. The experimental data in Figure 5a were collected from five SWCNT samples with different mean diameters between 1.17 and 1.38 nm.[23] Except for the hysteresis in the (10,10) SWCNT, we find that the simulations successfully reproduced the observed XRD measurements behavior and the ice-NT formation temperatures, T_m. In particular, the unusual diameter dependence of T_m, which increases with decreasing SWCNT diameter,[23] is well reproduced by the present simulations, as in the previous reports.[20,22]

On the basis of the MD simulations mentioned above, we calculated the polarization P along the SWCNT axis for the three SWCNT systems in a zero-electric field. The temperature dependence of P is shown in Figure 6. Here, P was calculated from the projection of each dipole moment of TIP3P water to the direction of SWCNT axis and taken as a time-average for 0.4 ns.[34] We find that the polarization for each of the three SWCNT systems maintains a constant value at low

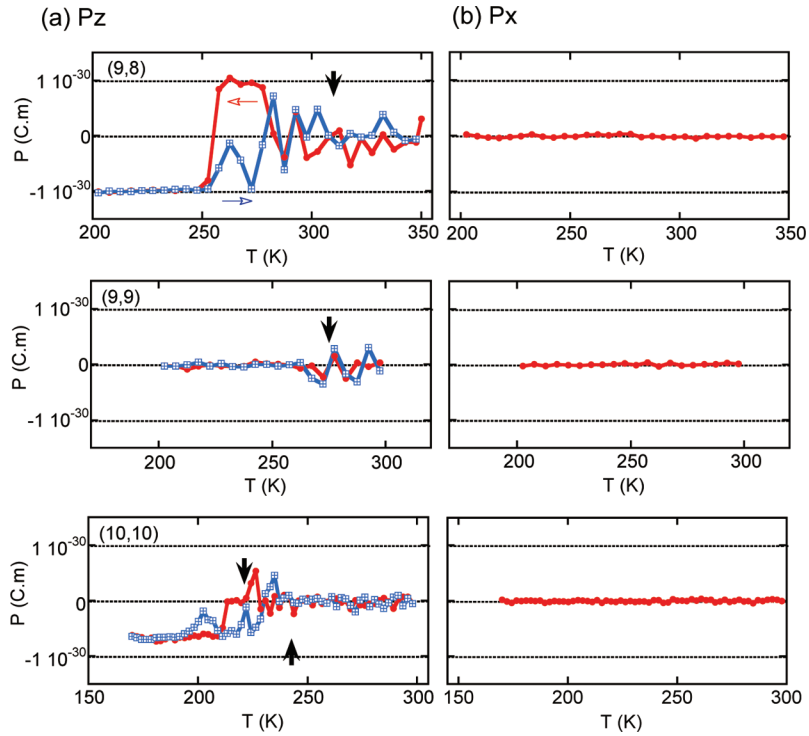

Figure 6. Temperature dependence of polarization, P, of water inside the (9,8), (9,9), and (10,10) SWCNTs from up to down in a zero-field. P is the polarization per water molecule averaged for 0.4 ns. (a) Polarization parallel to the SWCNT axis. (b) Polarization perpendicular to the SWCNT axis. The closed circles were taken while lowering temperature and the squares were taken with rising temperature. The arrows indicate the onset temperatures defined in Figure 5.

temperatures while it substantially fluctuates around T_m for the (9,8) and (9,9) SWCNTs. In contrast, for the thicker (10,10) SWCNT, the fluctuation is less remarkable and shows apparent hysteresis. The larger fluctuation observed in the narrower SWCNT systems likely originates in the quasi-one-dimensional nature of ice-NT structures. The polarization perpendicular to the SWCNT axis, P_x, was also examined as shown in Figure 6b. Compared to the parallel polarization, it is found that the perpendicular polarizations exhibit little fluctuation over the entire temperature range examined, including both above and below T_m. The large fluctuation along the SWCNT axis implies that the fluctuation is related to ordering of the O−H direction in water molecules along the SWCNT axis.

For parallel polarization at the lowest temperatures, the hexagonal ice-NT inside the (9,9) SWCNT has nearly zero polarization while the pentagonal and heptagonal ice-NTs have finite polarization. This implies that the pentagonal and heptagonal ice-NTs are a kind of ferroelectric with spontaneous polarization. The values per each *polygonal water ring*, that is, the polarization per five water molecules for the pentagonal ice-NT and per seven water molecules for the heptagonal ice-NT, are the same for the pentagonal and heptagonal ice-NTs: 5.0×10^{-30} C · m/ring = 1.5 debye/ring. From the corresponding snapshot structures, we find that each water chain, consisting of ice-NT structures, is proton-

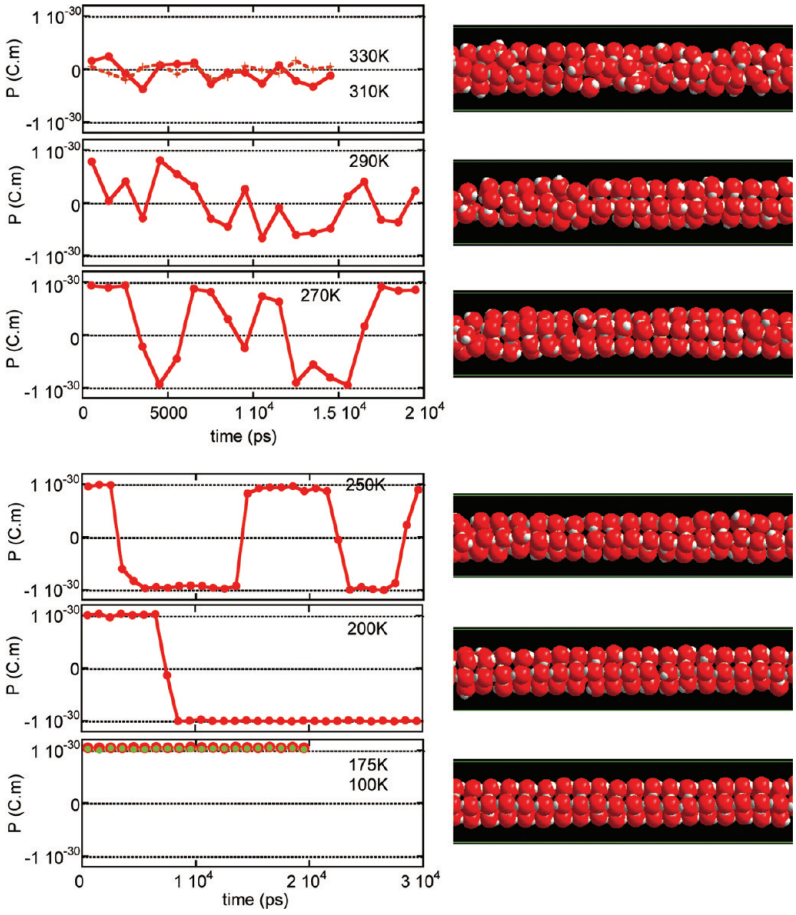

Figure 7. Time dependence of polarization, *P*, per water molecule in the (9,8) SWCNT. *P* is an average for 1 ns. At 200 K, *P* was not reversed for an additional 30 ns. Right: corresponding snapshot structures.

ordered along the SWCNT axis with a single domain at the lowest temperatures in all cases. Besides, since the pentagonal (heptagonal) ice-NT consists of *three (four)* positive ferroelectric chains and *two (three)* negative ferroelectric chains, it is "ferroelectric" or "ferrielectric" with a net polarization. On the other hand, the hexagonal ice-NT is found to be "anti-ferroelectric", because it has *three* positive ferroelectric chains and *three* negative ferroelectric chains with respect to the SWCNT axis. These low temperature structural features are consistent with the previous results calculated for TIP4P water inside SWCNTs.[26]

Even after a single domain with a net polarization develops inside the SWCNTs with lowering temperature, however, the direction of the polarization possibly fluctuates with time in a zero-field. In this context, we examined the time-dependence of the polarization for the (9,8) SWCNT system at constant temperature in detail. The results for parallel polarization are shown in Figure 7. *P* was taken as an average for 1.0 ns. Again, we find that the amplitude significantly fluctuates around $T_m = 310$ K. Below 270 K, the polarization shows nearly equal amplitude, but changes sign with time, $\pm P_0$. The corresponding snapshot structures indicate that inversion of the single domain ferroelectric occurs with time. With decreasing temperature, the inversion time τ increases steeply, and reaches roughly 60 μs at 150 K, 3.5 s at 100 K, and 10^{10} days at 50 K from extrapolation of τ at 200 K, 225 K (not shown in Figure 7), 250 K, and 270 K to lower temperatures assuming the Arrhenius law. The inversion time τ was also examined for the heptagonal ice-NT inside the (10,10) SWCNT. It was found that the inversion occurs down to 180 K below the ice-NT formation temperature of 220 K, within the MD simulation time scale of 100 ns. This is consistent with a previous NMR experiment,[25] which indicated that the large amplitude rotational motion of water molecules continues down to 120 K for a SWCNT sample with a mean diameter of 1.35 nm within the NMR time scale of 10^{-5} s.

While such net polarization seems to have been anticipated from the ice-NT structures and previous theoretical studies,[15] the present simulations for the finite systems indeed demonstrate that the ice-NTs can be really ferroelectric (or ferrielectric) or antiferroelectric with a *single domain* even at finite temperatures, despite the low dimensionality of the ice-NT structures.

We next discuss MD simulations of water encapsulated inside SWCNTs in an external electric field along the SWCNT axis. The polarization at 100 K is shown in Figure 8 for the (9,8), (9,9), and (10,10) SWCNT systems as a function of the electric field strength. The field was changed stepwise, and the polarization along the SWCNT axis was taken as a time-average for 0.1 ns after annealed for 0.4 ns at each field. We find a strong ferroelectric-like hysteresis loop for all the systems. However, comparing with the conventional ferroelectric loop, it exhibits a stepwise behavior. Combined with structural inspections it is found that the inversion of the ferroelectric-water-chain occurs at each step in polarization one by one. Therefore, the ice-NTs may have six different values for *P* in pentagonal ice-NT, seven in hexagonal ice-NT, and eight in heptagonal ice-NT in the presence of an external field.

The temperature dependence was further investigated for the case of water inside the (9,8) SWCNT in detail. Figure 9b shows hysteresis loops at 100, 175, 200, 225 K. Above 200 K, the "remanence" polarization is that of the one-chain case, with $P_0 = 1 \times 10^{-30}$ C · m/H_2O. Assuming a closed packed hexagonal SWCNT lattice with a lattice constant of 1.5 nm, this corresponds to a remanence polarization of $P_0 \approx 0.77$ μC/cm^2. Although the hysteresis loop becomes smaller with rising temperature, the saturated polarization, $\geq 5P_0$, shows little temperature dependence below 200 K,

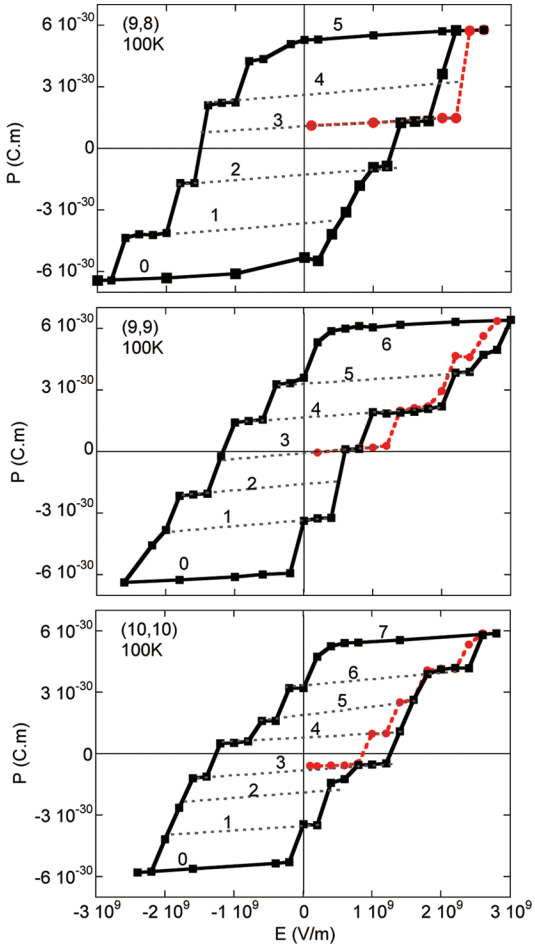

Figure 8. Hysteresis loops of polarization, *P*, per water molecule in the (9,8), (9,9), and (10,10) SWCNTs at 100 K. The electric field *E* was applied along the SWCNT axis. The closed circles are the initial polarization. The numbers denote the number of water chains whose ferroelectric polarization is parallel to the positive external electric field.

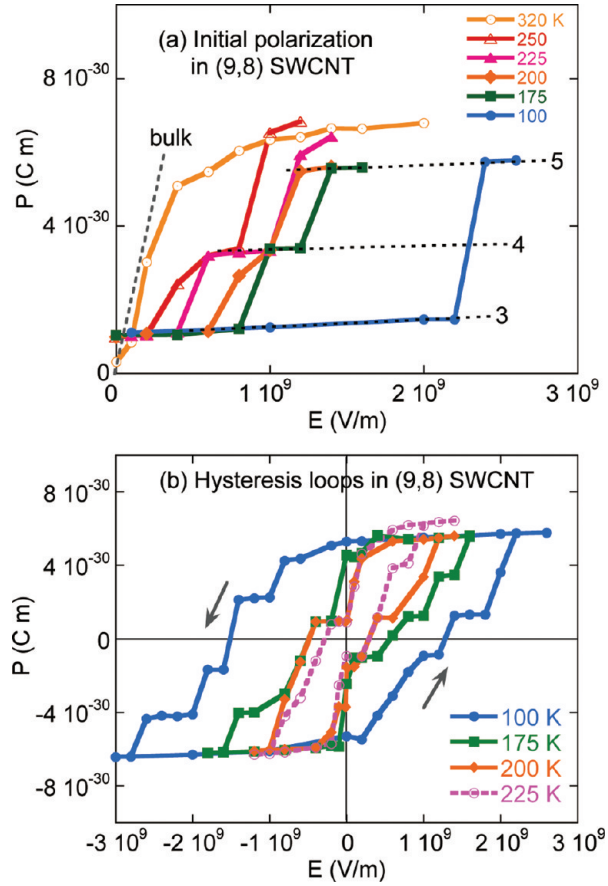

Figure 9. Hysteresis loops of polarization and initial polarization, *P*, per water molecule in the (9,8) SWCNT at several temperatures. The electric field *E* was applied along the SWCNT axis. The dotted line indicates extrapolation from bulk water at the low field limit. The numbers denote the number of water chains aligned to the electric field.

due to full inversion of the ferroelectric chains along the external field direction. The saturated polarization has the same order of magnitude as that of typical proton order−disorder type ferroelectrics, such as 4.73 μC/cm^2 for KH_2PO_4. On the other hand, the hysteresis width, corresponding to the field strength to reverse one chain, becomes weaker with rising *T*. Thus, distinct polarized states would be attained by quenching of the high temperature states polarized by the weaker field to lower temperatures.

Figure 9a depicts the initial polarization process for the (9,8) SWCNT. The solid straight line is the extrapolated polarization of bulk water to a higher field using a dielectric constant at the low field limit $\varepsilon_s \approx 71$ at 320 K. We find that the initial slope of the polarization curve at 320 K is closely described by this bulk limit, suggesting that the liquid water inside the (9,8) SWCNT shows roughly the same dielectric properties as for bulk water. At lower temperatures below T_m, the polarization process is quite different from that for bulk water, wherein stepwise polarization is clearly seen, as mentioned previously.

The saturated polarization, P_s, increases above 225 K in ice-NTs and approaches the value for TIP3P water, $P_w = 2.35$ debye $= 7.83 \times 10^{-30}$ C·m. This is because the strong electric field deforms the ice-NT structures; the electric dipole moment of each water molecule tends to align along the field direction, while at zero-field, the dipole moment of each molecule in the ice-NTs is not ex-

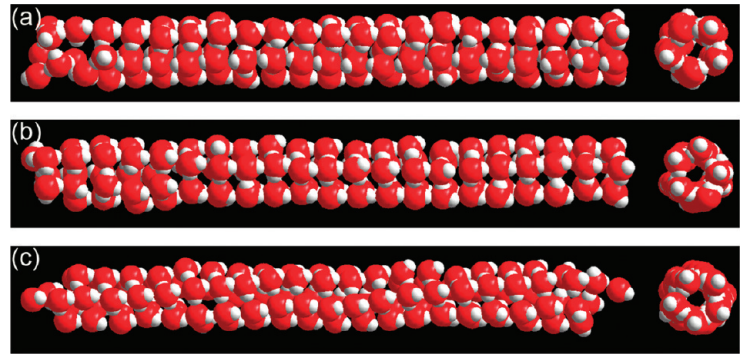

Figure 10. Snapshot structures of water inside the (9,8) SWCNT at 225 K in the external electric field along the SWCNT axis: (a) zero-field; (b) 1 × 10^9 V/m; (c) 1.4 × 10^9 V/m.

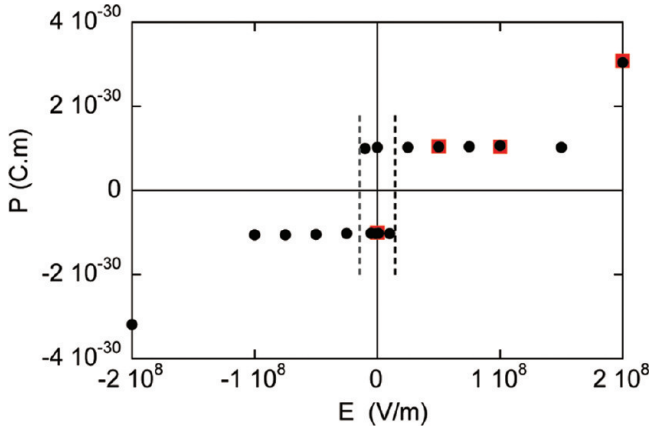

Figure 11. Field-cooled polarization, *P*, per water molecule at 200 K in the (9,8) SWCNT. The external field *E* was applied along the SWCNT axis. Above $E \approx 2 \times 10^7$ V/m, the spontaneous polarization of pentagonal ice-NT is aligned to the applied field.

actly parallel to the SWCNT axis. Distorted ice-NT structures are shown in the examples in Figure 10.

Finally, we discuss a cooling effect in an external electric field. Detailed simulations were performed for the (9,8) SWCNT system. In a given external field up to 2×10^8 V/m along the SWCNT axis, the system was cooled at a rate of 12.5 K/ns or 50 K/ns from 300 to 200 K. In all the cases examined, the formation of pentagonal ice-NT was observed. One of the interesting and important observations in this simulation is the polarization at low temperatures after the field cooling, indicated in Figure 11 as a function of the external field. In zero-field cooling, the polarization at 200 K randomly takes two possible polarization directions for several runs; positive (parallel) or negative (antiparallel) to the SWCNT axis. With cooling under fields above 2×10^7 V/m, it is confirmed that polarization of the ice-NT along the field direction can be achieved.

CONCLUSIONS

We have investigated the dielectric properties of water encapsulated inside three different diameter SWCNTs with finite length by means of classical molecular dynamics (MD) calculations using the TIP3P model for water. Within the present model, it was shown that the ice-NTs are novel dielectric materials with nanometer-scale dimensions. First, it was confirmed that the present MD simulations in a zero-external electric field could reproduce reported X-ray diffraction experiments. From a comparison, it was strongly suggested that ice-NTs consisting of more than 20 polygon units are indeed formed inside real SWCNTs. The calculated polarization indicates significant fluctuation with time and space around the phase transition temperature T_m. The fluctuation was more remarkable for thinner SWCNTs and for parallel polarization with respect to the SWCNT axis. Therefore, it was ascribed to quasi-one-dimensional fluctuations in the ice-NT structures. With reduced temperatures well below T_m, a ferro- or antiferro-electric single domain is formed inside the SWCNTs; although the polarization fluctuates between negative and positive polarity with the same magnitude in the intermediate temperature region, it finally freezes along one direction of the SWCNT axis. The polarization as a function of the external field indicated novel hysteresis behavior that cannot be observed in the bulk. The results predict that ice-NTs can be the world's smallest ferroelectrics with different polarized states, as small as 2 nm in diameter and shorter than 4 nm in length. The present findings suggest potential applications of SWCNTs encapsulating dielectric materials to fabricate the smallest ferroelectric devices.

METHODS

Classical molecular dynamics (MD) calculations were performed on water encapsulated in fixed SWCNTs with the indexes (9,8), (9,9), and (10,10) using the software package Materials Explorer 5.0 (Fujitsu Ltd.). The water molecule was described by the TIP3P model. The interaction potential, V_{WW}, among TIP3P molecules is the sum of the Lennard-Jones (LJ) potential, V_{LJ}, of the oxygen atoms and the Coulomb interaction potential, $V_{Coulomb}$, of the point charges between different TIP3P molecules:

$$V_{WW} = V_{LJ} + V_{Coulomb},$$
$$V_{LJ} = \sum_{i \neq j} 4\varepsilon_{OO}\left\{\left(\frac{\sigma_{OO}}{r_{ij}}\right)^{12} - \left(\frac{\sigma_{OO}}{r_{ij}}\right)^{6}\right\}, \quad (4)$$
$$V_{Coulomb} = \sum_{l \neq m} \frac{1}{4\pi\varepsilon_0}\frac{q_l q_m}{r_{lm}}$$

Here, r_{ij} is the oxygen(O)−oxygen(O) distance, ε_{OO} and σ_{OO} are LJ parameters for O−O interaction, r_{lm} is the distance between point charges q_l and q_m in different molecules, and ε_0 is the dielectric constant of vacuum. The interaction potentials of TIP3P water with carbon atoms in a SWCNT and artificial atoms are LJ potentials with LJ parameters ε_{OC}, σ_{OC}, and ε_{OA}, σ_{OA}, respectively. The LJ parameters used are $\varepsilon_{OO}/k_B = 76.6$ K, $\sigma_{OO} = 3.15061$ Å, $\varepsilon_{OC}/k_B = 46.3$ K, $\sigma_{OC} = 3.27531$ Å, $\varepsilon_{OA}/k_B = 5.3$ K, and $\sigma_{OA} = 2.75$ Å, where k_B is the Boltzmann constant.

The cutoff length in these interactions was set to 2.0 nm. Periodic boundary conditions are not applied to the systems with fixed volume and number of molecules, to obtain the results for finite systems. The temperature was controlled by a velocity-scaling method. The integration is carried out using the Gear algorithm with a time step of 1.0 fs.

Acknowledgment. This work was supported in part by a Grant-in-Aid for Scientific Research by the Ministry of Education, Culture, Sports, Science and Technology of Japan.

REFERENCES AND NOTES

1. Petrenko, V. F.; Whiteworth, R. W. *Physics of Ice*; Oxford Univ. Press: New York, 1999.
2. Buch, V., Devlin. J. P., Eds. *Water in Confining Geometries*; Springer-Verlag: Berlin, 2003.
3. Iijima, S.; Ichihashi, T. Single-Shell Carbon Nanotubes of 1-nm Diameter. *Nature (London)* **1993**, *363*, 603–605.

4. Bethune, D. S.; Klang, C. H.; De Vries, M. S.; Gorman, G.; Savoy, R.; Vazquez, J.; Beyers, R. Cobalt-Catalysed Grown Carbon Nanotubes with Single-Atomic-Layer Walls. *Nature (London)* **1993**, *363*, 605–607.
5. Maniwa, Y.; Kumazawa, Y.; Saito, Y.; Tou, H.; Kataura, H.; Ishii, H.; Suzuki, S.; Achiba, Y.; Fujiwara, A.; Suematsu, H. Anomaly of X-ray Diffraction Profile in Single-Walled Carbon Nanotubes. *Jpn. J. Appl. Phys.* **1999**, *38*, L668–L670.
6. Maniwa, Y.; Kataura, H.; Abe, M.; Suzuki, S.; Achiba, Y.; Kira, H.; Matsuda, K. Phase Transition in Confined Water inside Carbon Nanotubes. *J. Phys. Soc. Jpn.* **2002**, *71*, 2863–2866.
7. Maniwa, Y.; Matsuda, K.; Kyakuno, H.; Ogasawara, S.; Hibi, T.; Kadowaki, H.; Suzuki, S.; Achiba, Y.; Kataura, H. Water-Filled Single-Wall Carbon Nanotubes as Molecular Nanovalves. *Nat. Mater.* **2007**, *6*, 135–141, and in the supporting online materials.
8. Sekhaneh, W.; Kotecha, M.; Dettlaff-Weglikowska, U.; Veeman, W. S. High Resolution NMR of Water Absorbed in Single-Wall Carbon Nanotubes. *Chem. Phys. Lett.* **2006**, *428*, 143–147.
9. Wang, H.-J.; Xi, X.-K.; Kleinhammes, A.; Wu, Y. Temperature-Induced Hydrophobic-Hydrophilic Transition Observed by Water Adsorption. *Science* **2008**, *322*, 80–83.
10. Striolo, A.; Chialvo, A. A.; Gubbins, K. E.; Cummings, P. T. Water in Carbon Nanotubes: Adsorption Isotherms and Thermodynamic Properties from Molecular Simulation. *J. Chem. Phys.* **2005**, *122*, 234712.
11. Byl, O.; Liu, J.-C.; Wang, Y.; Yim, W.-L.; Johnson, J. K.; Yates, J. T., Jr. Unusual Hydrogen Bonding in Water-Filled Carbon Nanotubes. *J. Am. Chem. Soc.* **2006**, *128*, 12090–12097.
12. Striolo, A.; Chialvo, A. A.; Cummings, P. T.; Gubbins, K. E. Simulated Water Adsorption in Chemically Heterogeneous Carbon Nanotubes. *J. Chem. Phys.* **2006**, *124*, 074710.
13. Marti, J.; Gordillo, M. C. Structure and Dynamics of Liquid Water Adsorbed on the External Walls of Carbon Nanotubes. *J. Chem. Phys.* **2003**, *119*, 12540–12546.
14. Hummer, G.; Rasaiah, J. C.; Noworyta, J. P. Water Conduction through the Hydrophobic Channel of a Carbon Nanotube. *Nature (London)* **2001**, *414*, 188–190.
15. Koga, K.; Gao, G. T.; Tanaka, H.; Zeng, X. C. Formation of Ordered Ice Nanotubes inside Carbon Nanotubes. *Nature (London)* **2001**, *412*, 802–805.
16. Bai, J.; Su, C.-R.; Parra, R. D.; Zeng, X. C.; Tanaka, H.; Koga, K.; Li, J.-M. *Ab initio* Studies of Quasi-One-Dimensional Pentagon and Hexagon Ice Nanotubes. *J. Chem. Phys.* **2003**, *118*, 3913–3916.
17. Hanasakia, I.; Nakatani, A. Hydrogen Bond Dynamics and Microscopic Structure of Confined Water inside Carbon Nanotubes. *J. Chem. Phys.* **2006**, *124*, 174714.
18. Agrawal, B. K.; Singh, V.; Pathak, A.; Srivastava, R. *Ab initio* Study of Ice Nanotubes in Isolation or inside Single-Walled Carbon Nanotubes. *Phys. Rev. B* **2007**, *75*, 195420.
19. Kurita, T.; Okada, S.; Oshiyama, A. Energetics of Ice Nanotubes and their Encapsulation in Carbon Nanotubes from Density-Functional Theory. *Phys. Rev. B* **2007**, *75*, 205424.
20. Shiomi, J.; Kimura, T.; Maruyama, S. Molecular Dynamics of Ice-Nanotube Formation inside Carbon Nanotubes. *J. Phys. Chem. C* **2007**, *111*, 12188–12193.
21. Bai, J.; Wang, J.; Zeng, X. C. Multiwalled Ice Helixes and Ice Nanotubes. *Proc. Natl. Acad. Sci. U.S.A.* **2006**, *103*, 19664–19667.
22. Takaiwa, D.; Hatano, I.; Koga, K.; Tanaka, H. Phase Diagram of Water in Carbon Nanotubes. *Proc. Natl. Acad. Sci. U.S.A.* **2008**, *105*, 39–43.
23. Maniwa, Y.; Kataura, H.; Abe, M.; Udaka, A.; Suzuki, S.; Achiba, Y.; Kira, H.; Matsuda, K.; Kadowaki, H.; Okabe, Y. Ordered Water inside Carbon Nanotubes: Formation of Pentagonal to Octagonal Ice-Nanotubes. *Chem. Phys. Lett.* **2005**, *401*, 534–538.
24. Kolesnikov, A. I.; Zanotti, J.-M.; Loong, C.-K.; Thiyagarajan, P.; Moravsky, A. P.; Loutfy, R. O.; Burnham, C. J. Anomalously Soft Dynamics of Water in a Nanotube: A Revelation of Nanoscale Confinement. *Phys. Rev. Lett.* **2004**, *93*, 035503.
25. Matsuda, K.; Hibi, T.; Kadowaki, H.; Maniwa, Y.; Kataura, H. Water Dynamics inside Single-Wall Carbon Nanotubes: NMR Observations. *Phys. Rev. B* **2006**, *74*, 073415.
26. Luo, C.; Fa, W.; Zhou, J; Dong, J.; Zeng, X. C. Ferroelectric Ordering in Ice Nanotubes Confined in Carbon Nanotubes. *Nano Lett.* **2008**, *8*, 2607–2612.
27. Maniwa, Y.; Kataura, H.; Abe, M.; Fujiwara, A.; Fujiwara, R.; Kira, H.; Tou, H.; Suzuki, S.; Achiba, Y.; Nishibori, E.; Takata, M.; Sakata, M.; Suematsu, H. C_{70} Molecular Stumbling inside Single-Walled Carbon Nanotubes. *J. Phys. Soc. Jpn.* **2003**, *72*, 45–48.
28. Matsuda, K.; Maniwa, Y.; Kataura, H. Highly Rotational C_{60} Dynamics inside Single-Walled Carbon Nanotubes: NMR Observations. *Phys. Rev. B* **2008**, *77*, 075421.
29. Rols, S.; Cambedouzou, J.; Chorro, M.; Schober, H.; Agafonov, V; Launois, P.; Davydov, V.; Rakhmanina, A. V.; Kataura, H.; Sauvajol, J.-L. How Confinement Affects the Dynamics of C_{60} in Carbon Nanopeapods. *Phys. Rev. Lett.* **2008**, *101*, 065507.
30. Neria, E.; Fischer, S.; Karplus, M. Simulation of Activation Free Energies in Molecular Systems. *J. Chem. Phys.* **1996**, *105*, 1902–1921.
31. Jorgensen, W. L.; Chandrasekhar, J.; Madura, J. D.; Impey, R. W.; Klein, M. L. Comparison of Simple Potential Functions for Simulating Liquid Water. *J. Chem. Phys.* **1983**, *79*, 926–936.
32. Preliminary MD calculations were also performed for 103 and 105 water molecules inside the (9,8) SWCNT in zero-field. The results were essentially the same as the case for 104 water molecules presented in this paper.
33. Gnutzmann, V.; Vogel, W. Structural Sensitivity of the Standard Pt/SiO_2 Catalyst EuroPt-1 to H_2 and O_2 Exposure by *in situ* X-ray Diffraction. *J. Phys. Chem.* **1990**, *94*, 4991–4997.
34. The polarization *P* for all the water molecules inside SWCNTs, including the edge water molecules, was calculated, and the averaged value per water molecule was obtained.